Measurements of the wake from a floating tidal energy platform

Maricarmen Guerra, Alex E. Hay, and Benjamin Troncoso

Abstract—**In this investigation we present field observations of the combined wake generated by the four-turbine array mounted onboard Sustainable Marine Energy Canada PLAT-I 4.63. Measurements were conducted downstream of the platform in Grand Passage, a tidal channel in the southwest of the Bay of Fundy in eastern Canada. Velocity data were obtained by a vessel-mounted Acoustic Doppler Current Profilers (ADCP). Data were collected during peak flood and a receding ebb tide. The collected data were organized according to the turbine inflow velocity for ebb and flood tide. For each tide, the wake and undisturbed flow regions to the sides of the wake were identified. Vertical profiles of velocity in the wake were compared with measurements in the undisturbed flow to the sides of PLAT-I wake and to inflow velocity measured by a current-meter onboard PLAT-I. In all measurements the PLAT-I wake manifests as a reduction in flow speed at the depths spanned by the turbine rotors. The reduction is maximum near the platform for both ebb and flood. For flood, velocity profiles vertically mix less than 5 effective diameters downstream of the array, but velocities remain slower compared to the flow outside of the wake. Flow speed increases downstream, recovering approximately about 20 effective diameters from the platform.**

Index Terms—**Tidal energy, turbine wake, ADCP, field measurements.**

I. Introduction

CURRENT tidal energy projects consider the installation of hydrokinetic turbines directly into the flow. It is well-known that a wake forms downstream of these immersed turbines. The wake is a cone-shaped region characterized by slower velocities, because momentum is extracted from the flow, and by increased turbulent intensity, due to drag and eddy shedding from the rotor shaft and the rotating turbine blades. Wake measurements are critical for quantifying the hydrodynamic impacts of turbine presence and tidal energy extraction on the tidal flow. Wake extent and possible recovery are also relevant for turbine array design and placement.

This work was funded by the Offshore Energy Research Association, the Canada Foundation for Innovation, and the Natural Resources Canada Clean Growth Program.

M. Guerra is with the Department of Civil Engineering at Universidad de Concepción and with Center for Oceanographic Research COPAS COASTAL, Barrio Universitario s/n, Concepción, Chile (e-mail: marguerra@udec.cl).

A. E. Hay is with Dalhousie University, Department of Oceanography, 1355 Oxford Street, Halifax, NS, B3H 4R2, Canada (e-mail: alex.hay@dal.ca).

B. Troncoso was with the Department of Civil Engineering at Universidad de Concepción, Barrio Universitario s/n, Concepción, Chile (e-mail: betroncoso@udec.cl).

Digital Object Identifier:
https://doi.org/10.36688/ewtec-2023-paper-284

Turbine wakes are typically assessed using numerical models and controlled laboratory experiments, with only a few field wake studies available in the literature [1]. A wide range of hydrodynamic (or CFD) numerical models are available to evaluate the wake of turbines [2]–[4]. These models typically differ on how the turbine or its effects are represented in the model with the actuator disk being the most common and relatively low-cost model [5]. There are also regional scale circulation models that incorporate the effect of multiple turbines as a sink of momentum in the equations of flow motion [6]. Wake laboratory experiments typically consider scaled versions of turbines or small arrays and are conducted in straight rectangular flumes under steady flow conditions [7]–[9]. Wake studies suggest the wake extent and recovery are controlled by the turbine configuration, and by the ambient flow conditions such as ambient turbulence, shear and proximity to surface and bottom boundaries [10], [11].

Very few wake studies of full-scale turbines in the field are available in the literature [12]–[14]. The wake of ORPC Rivgen turbine was measured in [14] using a free-drifting turbulence-resolving ADCP. The wake was was found to be persistent, with reduced velocities and elevated turbulence observed through the extent of the measurements. The freely-drifting ADCP method was extended in [15] to map the turbulent flow around Sustainable Marine Energy Canada (SMEC) PLAT-I 4.63 floating tidal energy platform in Grand Passage, one of the Bay of Fundy's tidal channels, in Nova Scotia, Canada. The combined wake of the four turbines mounted on-board PLAT-I was measured for a single tidal stage on ebb while the turbines were operating, reporting a maximum 26% velocity deficit relative to the wake of not-operational turbines when ambient flow velocities were about 2 $\mathrm{m{\cdot}s^{-1}}$.

A new field experiment was conducted in October 2020 aimed at characterizing the combined wake of the four turbines mounted on-board PLAT-I while they were operational during spring tides in Grand Passage. Velocity data were obtained by a suite of mobile Acoustic Doppler Current Profilers (ADCPs), both vessel-mounted and free-drifting. Data were collected during ebb and flood tides (and therefore with time-varying inflow velocity), and under different turbine operating conditions. In this paper, wake measurements obtained by the vessel-mounted ADCP collected on October 14 and 17 2020 are presented. These measurements occurred during peak flood and during a receding ebb while the turbines were operational [16]. Section II describes the study site, data collection and data analysis methods. Section III describes the observed

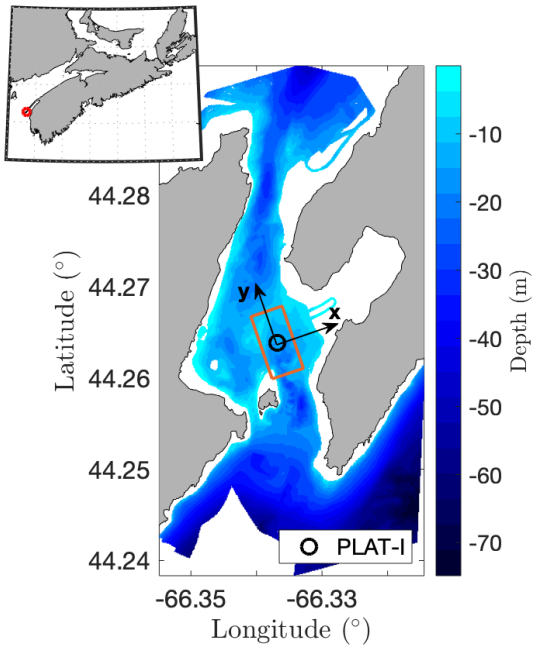

Fig. 1. a) Grand Passage map colored by bathymetry. The circle corresponds to PLAT-I location. The orange rectangle shows the measurements area. The (x, y) axis corresponds to the local coordinate system used through this study. The dark grey line corresponds to the coastline. Peter's Island is at the south entrance of Grand Passage (N 44.257°; W 66.338°).

wake. Finally conclusions are presented in Section IV.

II. Methods

A. Study Site

Wake measurements were conducted in Grand Passage, a tidal channel with strong currents (~3 m·s^{-1}). The channel is located on the southern side of the Bay of Fundy mouth, between Long and Brier islands, in Nova Scotia, Canada (N 44.27; W 66.34). The channel is oriented from north to south and it is about 1.5 km wide and 4 km long. Flood currents are northward, and in the opposite direction during ebb. Fig. 1 shows a map of Grand Passage, and the local coordinate system used in this investigation, defined to match the principal flow direction at the PLAT-I site (y-axis, 18.8° west of true north).The location of the tidal platform (PLAT-I) is shown with a black circle, and the orange rectangle corresponds to the field measurement area.

B. Tidal Energy Platform

PLAT-I 4.63 is a floating tidal energy platform developed by Sustainable Marine Energy Canada (SMEC). The three-hull floating platform is approximately 30 m long (center hull) and 30 m wide (cross-deck). An array of four Schottel Hydro SIT250 horizontal axis turbines is mounted on the platform's stern. Each SIT250 turbine is 6.3 m in diameter and rated at power 70 kW for a nominal speed of 2.7 m·s^{-1}, resulting in a total platform power of 280 kW [16]. The effective diameter of the array is 12.6 m. Turbine hub-depth is approximately 4.7 m below the free-surface. The platform is moored via a freely-rotating turret in the bow attached to a two-point mooring spread, and self-aligns with the flow [15], [16]. Through the tidal cycle, the platform rotates and the turbines face the flow at all-times, describing a circle of approximately 35 m radius centered in the main anchor point [15], [16]. The local coordinate system used in this investigation is centered at PLAT-I mooring location (N 44.2637°; W 66.3369°), and the turbines are located approximately at $y = 35$ m on flood, and at $y = -35$ m on ebb.

C. Data collection and processing

Water velocities were measured using a down-looking vessel-mounted 600 kHz RDI Workhorse Acoustic Doppler Current Profiler (ADCP). The ADCP was set to measure single-ping along-beam velocities at 1 Hz using 0.5 m depth cells and the first cell was located 2.6 m below the free-surface. Bottom-track velocities were recorded by the ADCP and were used to estimate water velocities in post processing. Obtained water velocities were then rotated to along and across-channel velocities in the local coordinate system shown in Fig. 1.

A synchronous Hemisphere GPS was installed on-board the vessel (Puffin, 18 ft) to record the ADCP position during the field experiments. Velocity profiles were collected along cross-wake transects at different distances downstream of PLAT-I. Data collection occurred on October 14, 2020 during the end of ebb tide, and on October 17, 2020, during peak flood. Both experiments occurred under mild wind conditions (less than 10 m·s^{-1}). In addition, turbine inflow speed was measured at 1 Hz using an electro-magnetic current-meter installed on-board PLAT-I just upstream of the turbines; these data were provided by SMEC.

Fig. 2 shows the trajectories followed by the research vessel while collecting data downstream of PLAT-I over a Google Earth image of Grand Passage. Ebb tide measurements are shown in blue and flood measurements are shown in orange. Individual transects were identified in post-processing, there were 51 cross-wake transects and 26 cross-wake transects on ebb. Velocity data were quality controlled by low echo-amplitude (35 dB) and low correlations (below 112.5 counts), wrapped velocity profiles were also removed from the dataset [17]. A corresponding inflow velocity (from the current-meter) was assigned to each identified transect based on the transect collection-time. The inflow velocity was later used to evaluate the velocity deficit in the wake. Figs. 3 and 4 show a time-series of the flow-speed measured by the current-meter together with an average flow speed measured by the ADCP during each transect. Ebb transects occurred after peak ebb, when turbine inflow speed was $\sim$ 1 m·s^{-1} (negative for ebb tide). Flood transects around peak flood when turbine inflow speed was between 1.75 m·s^{-1} and 2.25 m·s^{-1}.

D. Wake analysis

Each transect was analyzed to identify three regions: a disturbed flow region, or inner wake region, and two undisturbed flow regions well-outside of the wake, one

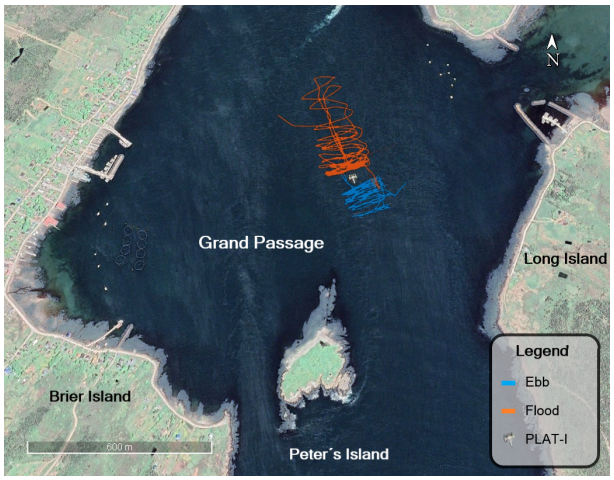

Fig. 2. Aerial view of Grand Passage at PLAT-I location from Google Earth. Flood tide vessel trajectories are shown by the orange lines, and ebb trajectories are shown by the blue lines. PLAT-I is seen inbetween the orange and blue lines.

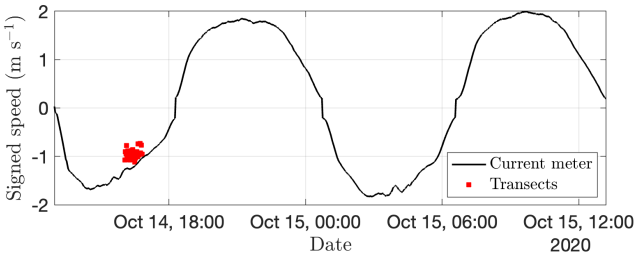

Fig. 3. Time-series of current meter signed speed, and transect timing plotted against average hub-depth flow speed for the ebb transects

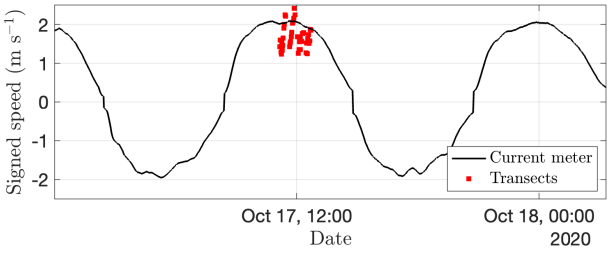

Fig. 4. Time-series of current meter signed speed, and transect timing plotted against average hub-depth flow speed for the flood transects

to the west and one to the east of the platform. The wake region was identified based on along-channel velocity through the transect, along-channel velocity at hub-depth and on the ADCP echo-amplitude data along the transect. Following this identification, averaged profiles of along-channel velocity were obtained within the wake and outside of the wake.

Fig. 5 shows an example of data from a single transect collected about 6 m downstream of the turbines (y = 41 m) during peak flood (current meter inflow speed 2.1 m·s^{-1}). Fig. 5a shows the along-channel velocity distribution along the transect (positive northward). On the west end of the transect (negative x) the along-channel velocity is approximately 2.5 m·s^{-1} in the upper water column, and slower near the bottom (black line), as expected for boundary layer flow. A sharp decrease in velocity is observed mid-transect

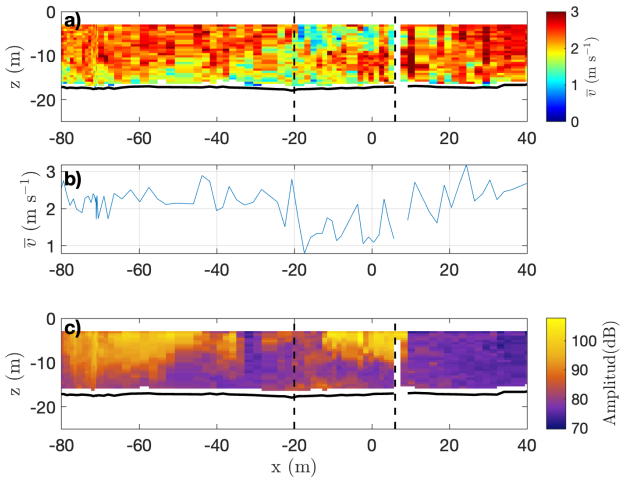

Fig. 5. Data from a single transect collected immediately downstream of the turbines: a) Along-channel velocity, b) Hub-depth along channel velocity, c) ADCP Echo-amplitude. Black line in a) and c) corresponds to the bottom (detected by the ADCP) and vertical dashed lines denote the wake approximate limits.

in the upper water column (-20 m <= x <= 5 m), corresponding to the wake. Mid-transect flow velocity decreases to about 1 m·s^{-1}. To the east (positive x), flow velocity rapidly increases to approximately 3 m·s^{-1}. Fig. 5b shows the hub-depth along-channel velocity along the transect, although variable, the velocity decrease is clear around x = 20 m. Fig. 5c shows the echo amplitude measured by the ADCP (corrected by spreading and attenuation). There are two regions of strong acoustic return. The strong returns observed to the west, are related to the wake of Peter's Island. The strong returns observed mid-wake correspond to air-entrainment from PLAT-I's wake and turbine rotation.

III. Results

A. Acoustic returns

Figs. 7 and 6 shows echo amplitude measured by the ADCP from ebb transects and flood transects respectively. During ebb, it is observed that the acoustic response is even in all measurements (70 to 75 dB) and only a few peaks are observed closer to the surface. The acoustic response is much higher during flood. A region of strong echo-amplitude is observed downstream of the turbines (corresponding to the wake) and decreases towards the east side (positive x). On the west side (negative x) there is a zone of elevated echo-amplitude related to the wake generated by Peter's Island. Data with maximum acoustic response correspond to areas with a high presence of particles that reflect the acoustic signal, in this case the particles correspond to bubbles generated by PLAT-I at the surface that are probably entrained by turbulent motions generated by turbine rotation.

B. Plan view of the wake

Following the methodology proposed in [15], transects were first grouped by their assigned inflow speed. Fig. 8 shows map of all the transects collected in both

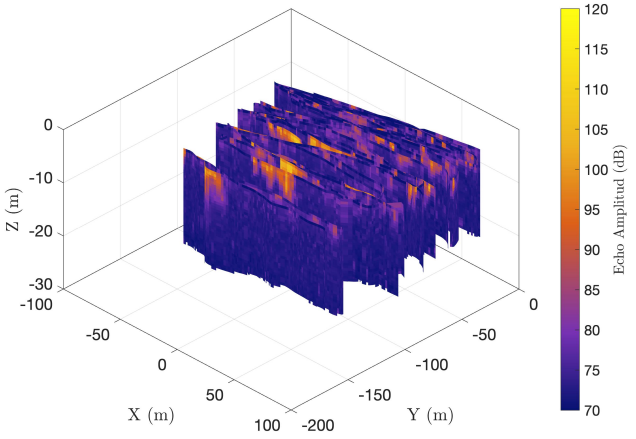

Fig. 6. Echo amplitude for all ebb transects.

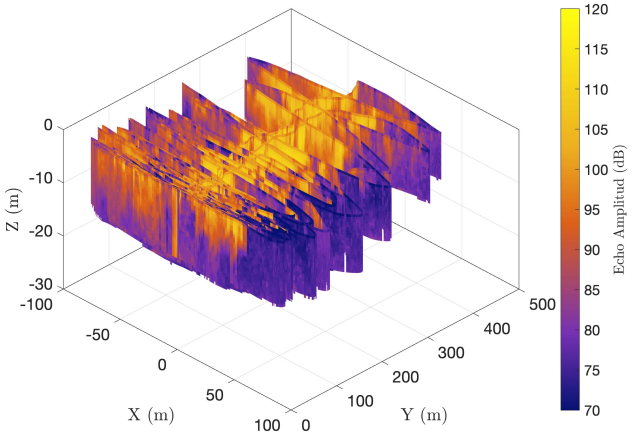

Fig. 7. Echo amplitude for all flood transects.

tidal conditions, colored by along-channel velocity at hub-depth in the local coordinate system. Fig. 8a shows data from all ebb transects, all of which occurred when the inflow speed (measured by the current meter) was $\sim$ 1 m·s^{-1}. Figs. 8b and c show flood data collected when inflow speed was between 1.75 m·s^{-1} and 2 m·s^{-1} and when inflow speed was above 2 m·s^{-1} respectively. The flood maps consistently show reduced velocities downstream of the turbines (around $X = 0$ m) compared to the velocity to the west and to the east of the platform, i.e. there is strong horizontal shear revealing the platform wake. When inflow speed is greater than 2 m·s^{-1}, the velocity reduction is greater as the undisturbed flow is much faster. On the contrary, no clear velocity decrease is observed at hub-depth downstream of the turbines data for this particular experiment.

C. Wake: Ebb tide

Fig. 9 shows the obtained average along-channel velocity profiles from a single ebb transect collected $\sim$ 25 m downstream of the turbines (less than 2 array equivalent diameters), when the turbine inflow speed was -1.25 m·s^{-1}. Reversed shear and small decrease in

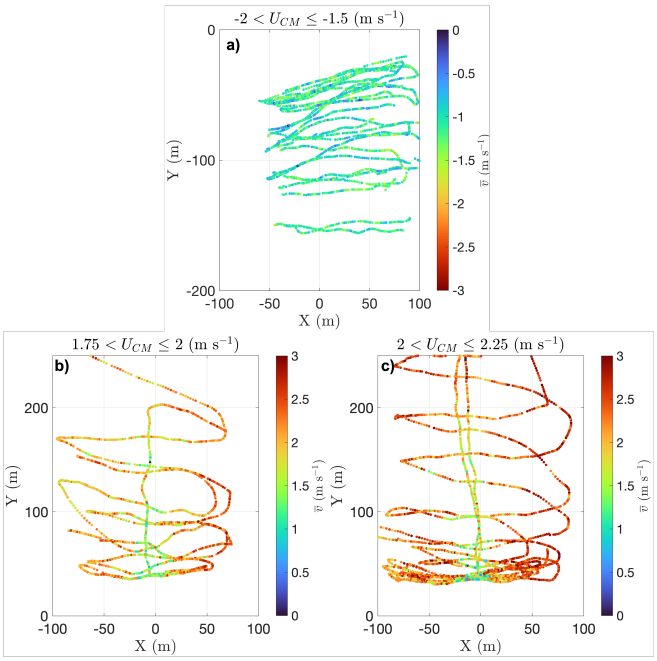

Fig. 8. Transect trajectory colored by hub-depth along-channel velocity: a) All ebb transects, b) All flood transects when inflow speed was between 1.75 m·s^{-1} and 2 m·s^{-1}, and c) All flood transects when inflow speed was above 2 m·s^{-1}.

velocity is observed in the inner wake profile at the depths spanned by the turbine rotors (-8 m $< z < -2$ m). For this particular transect, the difference between the inner wake along-channel velocity at hub-depth and the average out-of-wake along-channel velocity at hub-depth is $\sim$ 0.3 m·s^{-1} (28% velocity deficit). For this experiment, the wake was clearly detected in only 5 transects, all collected less than 60 m downstream of the turbines. Note that data collection occurred when turbine inflow velocities were low (around 1 m·s^{-1}). According to [16] turbines extract less than 5 kW when inflow speed is less than m·s^{-1}.

Fig. 10 shows the obtained velocity profiles for five transects where the wake was detected. Closer to the turbines, less than 30 m dowsnstream of the turbines, as shown before the wake manifests as a velocity decrease at the depths spanned by the turbine rotors (-8 m $< z < -2$ m). Hub-depth along-channel velocity is less than 1 m·s^{-1}. Further downstream, the wake was expanded vertically, the inner wake profiles vertically mix and the hub-depth velocity slightly increases. No recovery was observed in this set of measurements.

D. Wake: Flood tide

Fig. 11 shows the obtained average along-channel velocity profiles from the flood transect shown in Fig. 5. Out-of-wake profiles show the expected boundary-layer flow shape. The east profile (Fig.11a) shows a change in shear at $z \sim 10$ m, which might be related to Peter's island wake. Stronger velocities are observed to the east of the platform as previously shown in the maps. Fig. 11b shows the average along-channel velocity profile for the inner wake. Reversed shear and a sharp decrease in velocity is observed at the depths spanned by the turbine rotors (-8 m $< z < -2$ m), con-

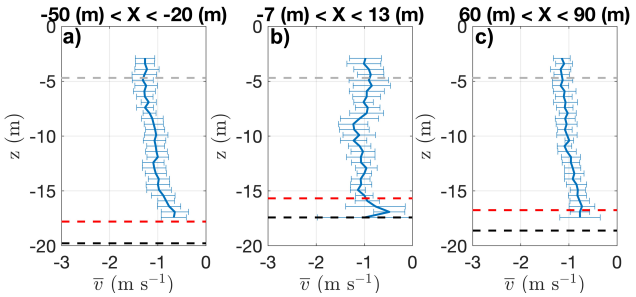

Fig. 9. Average along-channel velocity profiles obtained from an ebb transect collected 20 m downstream of the turbines: a) undisturbed flow to the west, b) inner wake, and c) undisturbed flow to the east of the platform. Horizontal blue lines correspond to $\overline{v} \pm \sigma_v$ for each transect region. Black dashed line corresponds to the bottom, and the red dashed line corresponds to the distance from the bottom affected by ADCP side lobe interference. Turbine hub-depth is shown by the grey dashed line.

trary to what is expected for boundary-layer flow. This velocity decrease corresponding to the wake generated by the turbines and energy extraction. The minimum velocity, 1.4 m·s^{-1}, is observed approximately at hub-depth. For this transect, the average out-of-wake along-channel velocity at hub-depth is $\sim$ 2.4 m·s^{-1}, thus a 40% velocity deficit is observed with respect to the undisturbed flow.

Fig. 12 shows the obtained averaged vertical profiles of along-channel velocity from selected transects that occurred when turbine inflow speed was above 2 m·s^{-1}. These profiles illustrate the evolution of the PLAT-I wake downstream of the turbines during flood. Close to the turbines (D_T less than 40 m, Fig. 12 top panels), the velocity decrease is clearly observed in the upper water column. As distance from the turbine increases (D_T between 65 m and 200 m, Fig. 12 mid panels), the wake expands vertically, the velocity profile vertically mixes, and velocity becomes homogeneous through the water column. Along-channel velocity increases with distances downstream, probably due to horizontal mixing with the surrounding flow, however, the flow is still much slower compared to the undisturbed flow outside of the PLAT-I wake. Farther downstream (D_T greater than 200 m), the inner wake profiles show the expected boundary-layer flow shape and are similar to the out-of-wake profiles, suggesting wake recovery.

IV. Conclusions and Future Work

This paper presents field measurements of the wake from SMEC PLAT-I tidal energy platform. The vessel-mounted ADCP transect method is proven to be suitable for capturing the wake at several distances downstream of the turbines. Since the only data available upstream of the turbines is single-point flow speed measured by a current-meter onboard PLAT-I, inner wake velocity profiles are compared to velocity profiles obtained well outside of the wake to the sides of PLAT-I to evaluate wake evolution and recovery.

The wake was detected for both ebb and flood tide. The ebb measurements occurred when turbine inflow speed was close to 1 m·s^{-1} (end of the ebb tide). For this slow flow case, the wake was detected up to 61 m (about 5 effective diameters) downstream of the array of turbines, but the velocity had not fully recovered at that distance.

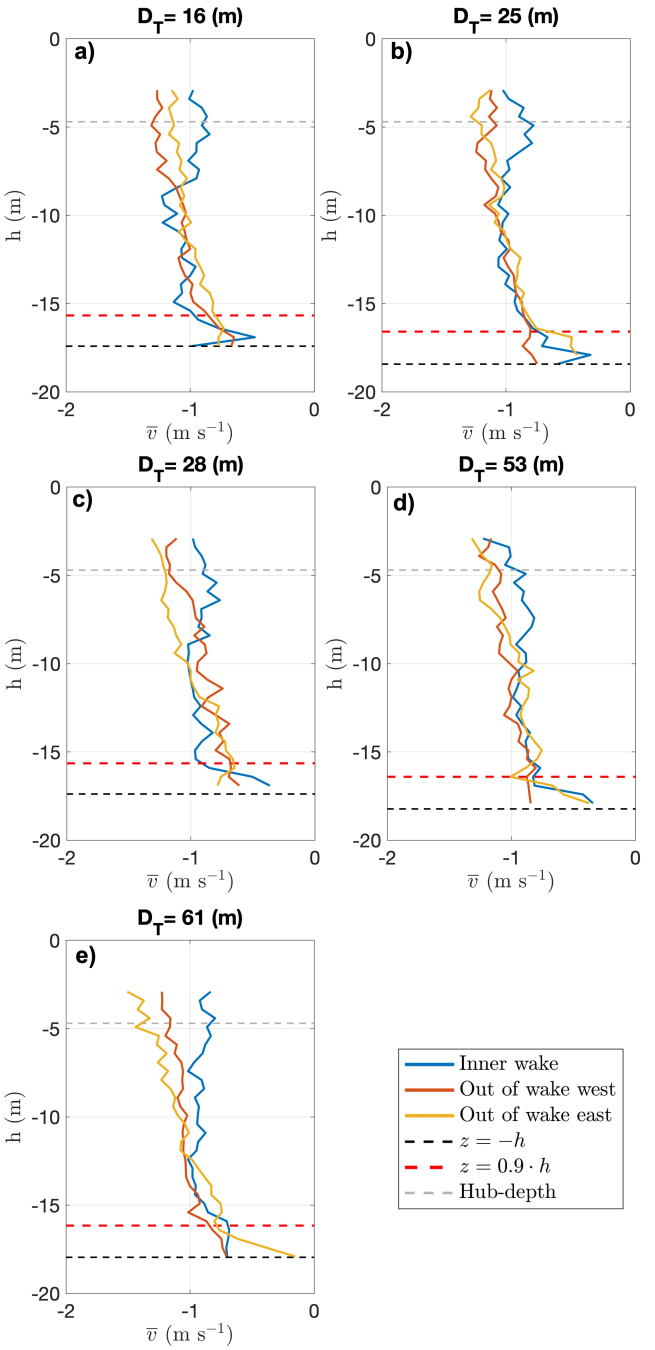

Fig. 10. Along-channel velocity profiles obtained from ebb transects at several distances downstream of the turbines (D_T). Blue profiles correspond to inner wake average profiles, and orange and yellow correspond to undisturbed flow average profiles to the west and to the east of the wake respectively.

The flood measurements occurred when inflow speed were about 2 m·s^{-1}, when turbines were extracting more power compared to the ebb measurements [16]. For this case the wake was detected farther downstream, and no wake was detected 20 effective diameters downstream of the turbines.

Future work includes evaluating of velocity deficit

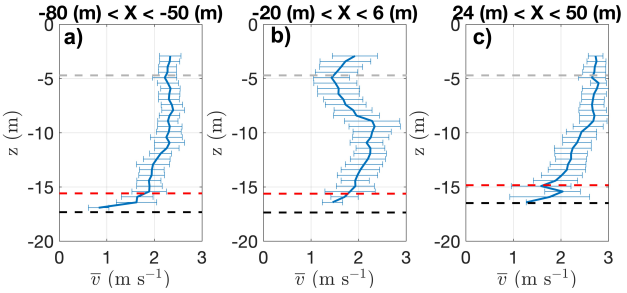

Fig. 11. Average along-channel velocity profiles obtained from the transect shown in Fig. 5: a) Out-of-wake west, b) inner wake, and c) out-of-wake east.

with respect to the current meter inflow speed, comparing these data with data collected prior to PLAT-I deployment, and further explore the wake of PLAT-I with data collected using drifting turbulence-resolving ADCPs as in [15].

Acknowledgement

The authors thank Greg Trowse, Richard Cheel, and the Luna Sea Solutions Inc. team for their constant help, support, and assistance with the experiments and data collection. The authors also thank the support and collaboration of Sustainable Marine Energy Canada, and the data they have provided. M. Guerra thanks the support of two MITACS Accelerated Postdoctoral fellowships in collaboration with Luna Sea Solutions Inc., and the support and funding of COPAS COASTAL ANID FB210021.

References

[1] C. M. Niebuhr, S. Schmidt, M. Van Dijk, L. Smith, and V. S. Neary, "A review of commercial numerical modelling approaches for axial hydrokinetic turbine wake analysis in channel flow," *Renewable and Sustainable Energy Reviews*, vol. 158, p. 112151, 2022.

[2] A. Olczak, T. Stallard, T. Feng, and P. Stansby, "Comparison of a RANS blade element model for tidal turbine arrays with laboratory scale measurements of wake velocity and rotor thrust," *Journal of Fluids and Structures*, vol. 64, pp. 87–106, 2016.

[3] D. D. Apsley, T. Stallard, and P. K. Stansby, "Actuator-line CFD modelling of tidal-stream turbines in arrays," *Journal of Ocean Engineering and Marine Energy*, vol. 4, no. 4, pp. 259–271, 2018.

[4] D. Gajardo, C. Escauriaza, and D. M. Ingram, "Capturing the development and interactions of wakes in tidal turbine arrays using a coupled bem-des model," *Ocean Engineering*, vol. 181, pp. 71–88, 2019.

[5] J. Sandoval, K. Soto-Rivas, C. Gotelli, and C. Escauriaza, "Modeling the wake dynamics of a marine hydrokinetic turbine using different actuator representations," *Ocean Engineering*, vol. 222, p. 108584, 2021.

[6] K. Soto-Rivas, D. Richter, and C. Escauriaza, "Flow effects of finite-sized tidal turbine arrays in the chacao channel, southern chile," *Renewable Energy*, vol. 195, pp. 637–647, 2022.

[7] S. Chawdhary, C. Hill, X. Yang, M. Guala, D. Corren, J. Colby, and F. Sotiropoulos, "Wake characteristics of a triframe of axial-flow hydrokinetic turbines," *Renewable Energy*, vol. 109, pp. 332–345, 2017.

[8] C. Gotelli, M. Musa, M. Guala, and C. Escauriaza, "Experimental and numerical investigation of wake interactions of marine hydrokinetic turbines," *Energies*, vol. 12, no. 16, p. 3188, 2019.

[9] S. Kang, Y. Kim, J. Lee, A. Khosronejad, and X. Yang, "Wake interactions of two horizontal axis tidal turbines in tandem," *Ocean Engineering*, vol. 254, p. 111331, 2022.

[10] P. Mycek, B. Gaurier, G. Germain, G. Pinon, and E. Rivoalen, "Experimental study of the turbulence intensity effects on marine current turbines behaviour. part i: One single turbine," *Renewable Energy*, vol. 66, pp. 729–746, 2014.

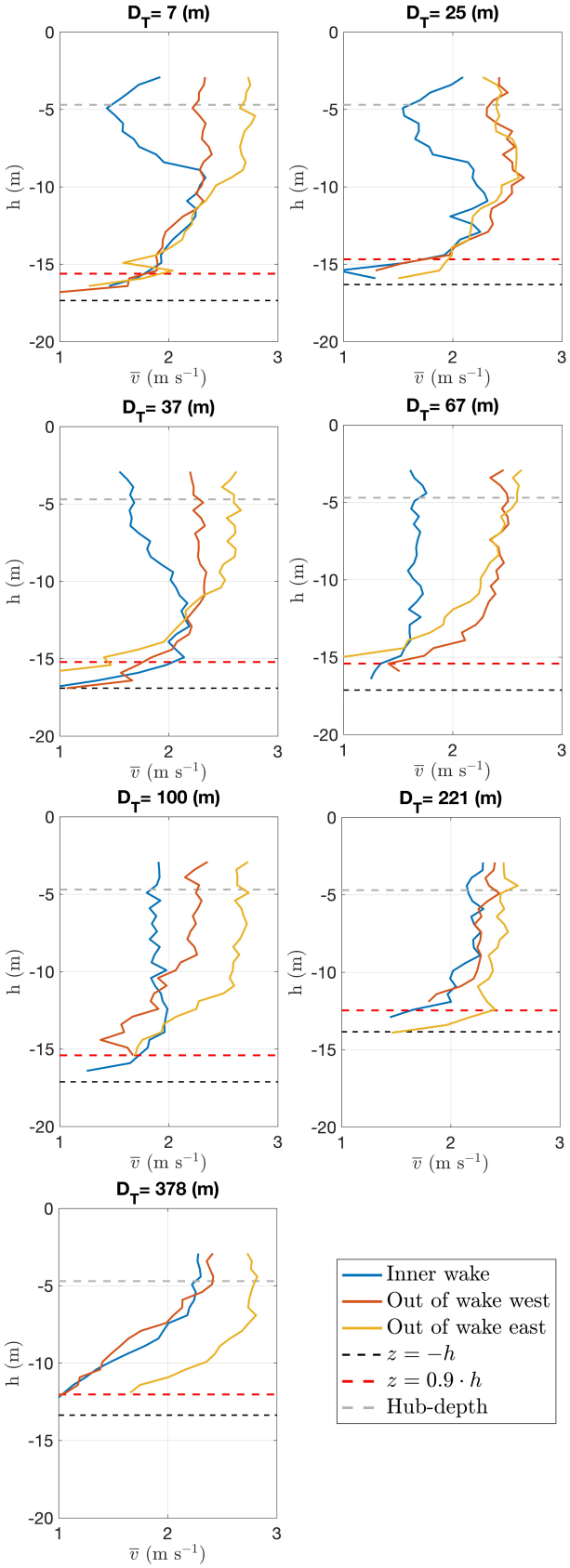

Fig. 12. Along-channel velocity profiles obtained from flood transects at several distances downstream of the turbines (D_T).

[11] T. Blackmore, W. Batten, and A. Bahaj, "Influence of turbulence on the wake of a marine current turbine simulator," *Proceedings of the Royal Society A*, vol. 470, no. 2170, p. 20140331, 2014.

[12] M. Rowell, M. Wosnik, J. Barnes, and J. P. King, "Experimental evaluation of a mixer-ejector marine hydrokinetic turbine at

two open-water tidal energy test sites in NH and MA," *Marine Technology Society Journal*, vol. 47, no. 4, 2013.

[13] B. Gunawan, J. Roberts, and V. Neary, "Hydrodynamic effects of hydrokinetic turbine deployment in an irrigation canal," in *Proc. of the 3rd Marine Energy Technology Symposium (METS2015), Washington, DC*, 2015.

[14] M. Guerra and J. Thomson, "Wake measurements from a hydrokinetic river turbine," *Renewable Energy*, vol. 139, pp. 483–495, 2019.

[15] M. Guerra, A. E. Hay, R. Karsten, G. Trowse, and R. A. Cheel, "Turbulent flow mapping in a high-flow tidal channel using mobile acoustic doppler current profilers," *Renewable Energy*, vol. 177, pp. 759–772, 2021. [Online]. Available: https://www.sciencedirect.com/science/article/pii/S0960148121008168

[16] R. Starzmann, N. Kaufmann, P. Jeffcoate, R. Pieroway, M. Guerra, and A. Hay, "Effect of fouling on the performance of an instream turbine," *International Marine Energy Journal*, vol. 5, no. 3, pp. 229–237, 2022.

[17] R. L. Gordon, "Acoustic doppler current profiler-principles of operation: A practical primer," *Rd Instruments*, vol. 54, p. 54, 1996.